IEEE Access
Multidisciplinary | Rapid Review | Open Access Journal

Received February 18, 2022, accepted March 4, 2022, date of publication March 14, 2022, date of current version May 12, 2022.

Digital Object Identifier 10.1109/ACCESS.2022.3159332

Feasibility Study of Practical AoA Estimation Using Compressed CSI on Commercial WLAN Devices

TAKERU FUKUSHIMA[1], (Member, IEEE), TOMOKI MURAKAMI[1], (Member, IEEE), HIRANTHA ABEYSEKERA[1], (Member, IEEE), TAKUYA FUJIHASHI[2], (Member, IEEE), TAKASHI WATANABE[2], (Member, IEEE), AND SHUNSUKE SARUWATARI[2], (Member, IEEE)

[1]Access Network Service Systems Laboratories, NTT Corporation, Yokosuka 239-0847, Japan
[2]Graduate School of Information Science and Technology, Osaka University, Osaka 565-0871, Japan

Corresponding author: Takeru Fukushima (takeru.fukushima.pr@hco.ntt.co.jp)

This work was supported by Japan Society for the Promotion of Science (JSPS) KAKENHI under Grant JP19H01101 and JP17KT0042, and JST PRESTO, Japan, under Grant PMJPR2032.

ABSTRACT Wireless local area network (WLAN)-based localization is key for advanced indoor Internet-of-Things and embedded sensor applications. To further improve the accuracy of indoor localization, attention has been focused on WLAN-based indoor localization using channel-state information (CSI) in addition to the existing information provided by received signal strength (RSS). For easy and low cost installation of wireless sensing, wireless sensing based on standardized protocols and commercial WLAN devices, such as IEEE 802.11ac and IEEE 802.11ax, is necessary. There are few papers demonstrating AoA estimation results by using commercial WLAN devices based on CSI. Therefore, we propose a practical method for estimating the AoA to solve four problems: 1) compressed CSI, which cannot be used for AoA estimation directly, 2) the antenna wireline, in which the phase changes depending on the length of the wireline, 3) the antenna spacing, in which the distance between antennas places a restriction on AoA estimation, and 4) antenna individuality, in which the antennas used in actual MIMO communication have different characteristics. We implemented the proposed method on IEEE 802.11ac devices and evaluated it in a lecture room and shield tent. The results indicate that the proposed method can estimate AoA with an average error of 9.1° and reduce the estimation error by 85.4 % compared with a straightforward approach.

INDEX TERMS Wireless sensing, angle-of-arrival estimation, IEEE 802.11ac, IEEE 802.11ax, compressed CSI.

I. INTRODUCTION

Wireless localization is a key technique for several important indoor Internet-of-Things (IoT) and embedded sensor applications such as navigation [1]–[4], location-aware services [5]–[7], and human–computer interaction [8]–[10]. The global positioning system [11] has become a standard technology for outdoor localization. However, indoor localization faces several challenges, and numerous studies have been conducted using technologies such as WLAN [12]–[20], RFID [21]–[24], Bluetooth [7], [25], [26], IEEE 802.15.4 [27]–[29], millimeter-wave [30], aircraft signals [31], ultrawideband [32], and backscatter signals [33].

The associate editor coordinating the review of this manuscript and approving it for publication was Kashif Saleem.

We focus on the WLAN-based estimation of the angle of arrival (AoA), which is a key piece of information of WLAN-based indoor localization, because it allows the existing WLAN infrastructure to acquire the AoA of WLAN packets. ArrayTrack is the first system to consider AoA derivation in the WLAN infrastructure and a proof-of-concept test was demonstrated using the Rice WARP FPGA platform [34]. Several WLAN-based wireless localization techniques [14], [15], [17]–[20] have been developed using channel state information (CSI) on IEEE 802.11n [35] with the CSI tool [36], [37]. In particular, Ubicarse [14], SpotFi [15], Chronos [17], MonoLoco [18], and UAT [19] can successfully acquire the AoA from the CSI tool for wireless localization. For example, Chronos [17] performs decimeter-level localization

by combining the AoA and time of flight of wireless signals.

The method of this paper advances WLAN-based AoA estimation a step further toward wide deployment as it allows commercial WLAN devices such as IEEE 802.11ac and IEEE 802.11ax to realize highly accurate AoA estimation. WLAN-based AoA estimation in previous studies was based on IEEE 802.11n (WLAN 4), CSI tool, Intel 5300 WLAN cards, Atheros chipsets, and WARP. To deploy WLAN-based localization in real environments, we must address how commercial WLAN devices such as IEEE 802.11ac (WLAN 5) and IEEE 802.11ax (WLAN 6) can yield AoA data.

To achieve AoA estimation on commercial IEEE 802.11ac and IEEE 802.11ax devices, we must solve the following four problems.

1) Compressed CSI problem: The AoA estimation system has to recover phase information from the CSI compression format standardized in IEEE 802.11ac and IEEE 802.11ax.
2) Antenna wireline problem: The phase changes depending on the length of the wireline between each antenna and the analog-to-digital (AD) converter.
3) Antenna spacing problem: It is desirable that the distance between adjacent antennas be $\lambda/2$ where λ is the wavelength of radio waves. However, the distance in several commercial WLAN devices is larger than $\lambda/2$ to improve the multiple-input multiple-output (MIMO) performance because of the need for a low spatial correlation among antennas.
4) Antenna individuality problem: It is desirable that the characteristics of the signals received by each antenna be the same. However, the antennas used in actual MIMO communication have different characteristics due to the effects of housing, circuit boards, and installation environments.

Details on the aforementioned four problems are provided in Section III.

To solve these four problems, this paper proposes the first AoA estimation method for IEEE 802.11ac and IEEE 802.11ax WLAN devices. The compressed CSI problem is solved by restoring the right singular matrix, which contains relative phase information among antennas, from compressed CSI. The antenna wireline problem is solved by calibrating the right singular matrix based on the right singular matrix for an AoA of zero degrees. The antenna spacing problem is solved by using a heuristic algorithm that estimates the number of times the phase is rotated by the AoA and distances between adjacent antennas that are larger than $\lambda/2$. The antenna individuality problem is solved by using another heuristic algorithm that selects a combination of antennas to reduce the AoA estimation error. Our solutions are detailed in Section IV. We evaluate the accuracy of the proposed method in a lecture room and shield tent. Compared with a straightforward approach, the proposed method reduced the AoA estimation error by 85.4 %.

The main contributions of the paper are as follows:

- We propose an AoA estimation method that is not for any specific Wi-Fi devices. The proposed method may be used not only IEEE 802.11n and IEEE 802.11ac but also for IEEE 802.11ax.
- The problems in achieving AoA estimation on IEEE 802.11ac and IEEE 802.11ax devices are identified. In particular, the antenna spacing problem is considered, wherein the antenna spacing of the access point exceeds half the wavelength of the radio wave for MIMO communication. In contrast, most previous studies assumed an antenna spacing of $\lambda/2$.
- In this study, the experimental settings include packet capture software and commodity IEEE 802.11ac devices, whereas previous studies employed CSI tool, Intel 5300 WLAN cards, Atheros chipsets, and WARP.
- The experimental evaluation shows that the proposed method can operate in actual environments. The average error of the method is approximately 10.18°, whereas that of the straightforward approach is approximately 62.6° in a lecture room. The average calculation time of the proposed method is approximately 0.6 s.

The rest of this paper is organized as follows. Section III introduces compressed CSI in IEEE 802.11ac and IEEE 802.11ax devices and identifies the problems created by using commercial WLAN devices for AoA estimation. Section IV describes the solutions based on the proposed method for the problems identified in Section III. Section V evaluates the performance of the proposed method in both a shield tent and a lecture room. Section II discusses related work, and finally, Section VI concludes this paper.

II. RELATED WORK

This paper is related to wireless sensing and AoA estimation.

A. WIRELESS SENSING

Studies on wireless sensing can be classified into three categories:

1) Direct use of a physical layer signal
2) Use of raw CSI
3) Use of compressed CSI following IEEE 802.11ac

Many studies on wireless sensing through the direct use of a physical layer signal have explored the many possibilities of wireless sensing, such as for device localization [38], [39], device-free user localization [40]–[42], device proximity detection [43], emotion recognition [44], gesture recognition [45], hidden electronics detection [46], human detection through walls [47]–[49], in-body device localization [50], respiratory monitoring [51], [52], heart rate monitoring [51], RF imaging, [48], [53], [54], and touch sensing [55]. For example, Vital-Radio [51] successfully tracked the breathing and heart rates of multiple users simultaneously even when the users were 8 m away from the wireless sensing device. However, the above methods have a deployment cost problem due to the need for special wireless devices such as USRP and millimeter-wave (mmWave) transceivers.

The use of raw CSI advances the possibility of actual implementation. The studies using raw CSI include device localization [14], [15], [17]–[19], activity recognition [56], [57], device-free user localization [58]–[60], device motion tracking [9], device-free motion tracking [61]–[63], gesture recognition [64], [65], human dynamics monitoring [66], keystroke recognition [67], material sensing [68], respiratory monitoring [52], object state change detection [69], and soil sensing [70]. For example, IntuWition [68] achieved an accuracy of 95 % in classifying copper, aluminum, plywood, birch, and humans. However, as the raw CSI is extracted through the use of highly specific hardware such as Intel 5300 NICs, Atheros chipsets, and WARP, raw-CSI-based wireless sensing methods cannot be implemented on other wireless LAN cards even if the card supports IEEE 802.11n.

The proposed method is classified as wireless sensing using compressed CSI. As described in III-B, compressed CSI is already applied in commercial IEEE 802.11ac and IEEE 802.11ax devices. Studies on compressed-CSI-based wireless sensing have recently begun. They include position estimation [71] and object detection [72].

B. AOA ESTIMATION

AoA estimation has been studied for military radars since the 1950s. In recent years, several studies on AoA estimation have examined its use in various applications such as beamforming to improve the performance of mobile communications and indoor localization. For example, ArrayTrack [12], Ubicarse [14], ToneTrack [16], SpotFi [15], Chronos [17], MonoLoco [18], UAT [19], and LocAP [20] have been employed for indoor localization, the authors of [73], [74] improved the throughput by using beamforming in massive MIMO for mmWave, and BreathTrack [75] has been employed for the tracking of human breath.

Two types of AoA estimation exist: those that use the received signal strength indicator (RSSI) and those that use phase. RSSI-based AoA estimation utilizes multiple RX antennas: the AoA is estimated by calculating the RSSI differences among the antennas. For example, ALRD [76] estimates the AoA using the fact that the difference in RSSI between antennas increases as the AoA increases from 0°. However, it is difficult to improve the accuracy of AoA estimation using RSSI when the influence of multipath propagation is large, as is true in indoor environments.

Phase-based AoA estimation uses the phase difference acquired by multiple antennas as described in Section II-B. Phase-based AoA estimation assumes that the distance between a TX antenna and an RX antenna is infinity, and all RX antennas in the same array have the same the AoA. Most of the existing studies on AoA estimation [14], [15], [17]–[20], [77]–[80] assume that the antenna arrays are linear, equally spaced, and that the distance between adjacent antennas is less than or equal to $\lambda/2$. Various methods have been proposed for estimating the AoA using phase, such as minimum variance distortionless response, MUSIC, and the estimation of signal parameters via rotational invariance techniques. However, this previous research is only available for 802.11n. These methods cannot be uses on commercial WLAN devices directly. Even if these methods are used, the compressed CSI, antenna wireline, antenna spacing, and antenna individuality problems described in Section III need to be addressed when using commercially available IEEE 802.11ac devices to estimate AoA.

Figure 1 illustrates the basis of AoA estimation using radio waves, where M is the number of antennas, θ is the AoA, and d is the antenna spacing. In Figure 1, all antennas form a uniform linear array with an equal spacing of d between adjacent antennas. When a radio wave transmitted from a TX antenna is received by multiple RX antennas, the path of the radio wave differs at the RX antenna depending on the AoA. As the phase observed at each RX antenna depends on the path length, the AoA can be estimated using the phase difference among the RX antennas.

If the TX antenna is sufficiently far from the RX antennas, we can assume that all the RX antennas receive the radio waves transmitted from the TX antenna at the same AoA. If all AoAs are equal, the phase difference between RX antenna i and RX antenna 1 can be expressed as follows.

$$h_i = 2\pi f \frac{d(i-1)\sin(\theta)}{c} \tag{1}$$

where h_i is the phase difference between RX antennas i and 1 ($i = 2, 3, \cdots, M$), f is the frequency of the radio wave, c is the speed of light, and $d(i-1)\sin(\theta)$ is the radio path difference yielded by the distance $d(i-1)$ between antenna i and antenna 1.

The CSI matrix at an arbitrary subcarrier can be expressed as follows when CSI is used in MIMO transmission in WLAN communication.

$$\mathbf{CSI} = \begin{pmatrix} \mathrm{csi}_{1,1} & \mathrm{csi}_{1,2} \cdots & \mathrm{csi}_{1,N} \\ \mathrm{csi}_{2,1} & \mathrm{csi}_{2,2} \cdots & \mathrm{csi}_{2,N} \\ \vdots & \ddots & \vdots \\ \mathrm{csi}_{M,1} & \mathrm{csi}_{M,2} \cdots & \mathrm{csi}_{M,N} \end{pmatrix} \tag{2}$$

where M is the number of RX antennas, and N is the number of TX antennas. $\mathbf{CSI}_{*,1}$, which is the CSI from the 1st TX antenna to M RX antennas, is expressed as:

$$\mathbf{CSI}_{*,1} = \begin{pmatrix} \mathrm{csi}_{1,1} \\ \mathrm{csi}_{2,1} \\ \vdots \\ \mathrm{csi}_{M,1} \end{pmatrix} = \begin{pmatrix} a_1 e^{j\Theta + j2\pi f \frac{0 \cdot d\sin(\theta)}{c}} \\ a_2 e^{j\Theta + j2\pi f \frac{1 \cdot d\sin(\theta)}{c}} \\ \vdots \\ a_M e^{j\Theta + j2\pi f \frac{(M-1) \cdot d\sin(\theta)}{c}} \end{pmatrix} \tag{3}$$

where Θ is the phase of RX antenna 1 and a_m is the amplitude of RX antenna m. $\widetilde{h_i}$, which is the observed phase difference between RX antenna 1 and RX antenna i, is expressed as follows.

$$\widetilde{h_i} = \arg\left(\frac{\mathrm{csi}_{i,1}}{\mathrm{csi}_{1,1}}\right) \tag{4}$$

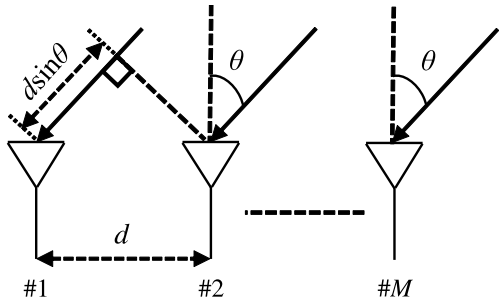

FIGURE 1. Basis of AoA estimation. Antenna array consists of M antennas, θ is AoA, and d is antenna spacing.

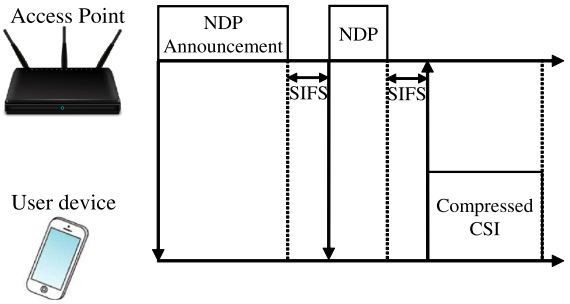

FIGURE 2. Frame sequence of compressed CSI. User device calculates compressed CSI using NDP frame from access point.

From Equation (1) and Equation (4), we can estimate θ using the phase difference among the RX antennas, as d, f, and c are known.

III. BACKGROUND AND PROBLEM IDENTIFICATION

A. CHALLENGES FOR AOA ESTIMATION USING IEEE 802.11AC AND IEEE 802.11AX WLAN DEVICES

The following four problems must be solved for the practical deployment of AoA estimation on IEEE 802.11ac and IEEE 802.11ax WLAN devices.

1) Compressed CSI problem
2) Antenna wireline problem
3) Antenna spacing problem
4) Antenna individuality problem

B. COMPRESSED CSI PROBLEM

It is generally known that the amount of CSI (frequency and antenna domains) for the transmit beamforming is extremely large. In IEEE 802.11ac, some compression techniques are specified to reduce the amount of CSI feedback [81]. Compressed CSI is a CSI feedback method specified in IEEE 802.11ac [81]. Two types of CSI feedback methods exist: implicit feedback and explicit feedback. Compressed CSI is classified as an explicit feedback method and it cannot be employed for AoA estimation directly because it contains only compressed information. Note that the CSI assumed in this paper has a center frequency offset and sampling frequency offset corrected by the preamble signals specified in WLAN.

Figure 2 shows the frame sequence for acquiring compressed CSI. The frame sequence is a type of WLAN communication between an access point and a user device. First, the access point transmits a null data packet announcement (NDPA) frame and a null data packet (NDP) frame to the user device. Second, the user device calculates compressed CSI from the NDP. Finally, the user device transmits compressed CSI to the access point.

Compressed CSI is calculated using singular value decomposition (SVD) and a Givens rotation on the CSI matrix [35]. The SVD of CSI is expressed as:

$$\mathbf{CSI} = \mathbf{USV}^H \tag{5}$$

where $\mathbf{U}$ is a left singular matrix, $\mathbf{S}$ is a diagonal matrix with singular values of CSI, and $\mathbf{V}$ is a right singular matrix. Compressed CSI is the angle information ϕ, ψ, which corresponds to $\mathbf{V}$ compressed using a Givens rotation. We can acquire as many as $\mathbf{V}$ subcarriers.

The following equation represents the relationship between matrix $\mathbf{V}$ and angle information ϕ, ψ calculated through a Givens rotation.

$$\mathbf{V} = \left\{ \prod_{k=1}^{\min(N,M-1)} \left[\mathbf{D}_k \prod_{l=k+1}^{M} \mathbf{G}_{l,k}^T(\psi_{k,k}) \right] \right\} \widetilde{\mathbf{I}}_{M\times N} \tag{6}$$

$\mathbf{D}_k$ is a diagonal matrix expressed as follows:

$$\mathbf{D}_k = \begin{pmatrix} \mathbf{I}_{k-1} & 0 & 0 & \cdots & 0 \\ 0 & e^{j\phi_{k,k}} & 0 & \cdots & 0 \\ 0 & 0 & \ddots & 0 & 0 \\ \vdots & \vdots & 0 & e^{j\phi_{M-1,k}} & 0 \\ 0 & 0 & 0 & 0 & 1 \end{pmatrix} \tag{7}$$

$\mathbf{G}_{l,k}(\psi)$ is a Givens rotation matrix expressed as

$$\mathbf{G}_{l,k} = \begin{pmatrix} \mathbf{I}_{k-1} & 0 & 0 & 0 & 0 \\ 0 & \cos(\psi) & 0 & \sin(\psi) & 0 \\ 0 & 0 & \mathbf{I}_{l-k-1} & 0 & 0 \\ 0 & -\sin(\psi) & 0 & \cos(\psi) & 0 \\ 0 & 0 & 0 & 0 & \mathbf{I}_{M-1} \end{pmatrix} \tag{8}$$

where $\mathbf{I}_{k-1}$ is a $(k-1)\times(k-1)$ identity matrix, and $\widetilde{\mathbf{I}}_{M\times N}$ is an identity matrix in which zeros are inserted as the missing elements if $N \neq M$.

An example of data reduction by compressed CSI is as follows. Let us assume that there are 4 TX antennas, 2 RX antennas, and 52 subcarriers. To extract the CSI, first input the obtained compressed value of the CSI into Equations (7) and (8). Next, the CSI is restored by inputting the calculated value into Equation 6. To extract the CSI, first input the obtained compressed value of the CSI into Equations (7) and (8). Next, the CSI is restored by inputting the calculated value into Equation (6).

To investigate the amount of data reduction, this study compares the data size of compressed CSI with that of the

CSI matrix. CSI consists of signal amplitude and phase information. The signal to noise ratio (SNR) is given as 8 bits per RX antenna. The CSI information specified by IEEE 802.11ac contains the amplitude and I/Q signals per subcarrier. The amplitude is 3 bits. The I/Q signals are multiplied by the number of TX antennas and the number of RX antennas, and each I signal and Q signal is 8 bits. Therefore, the total data size of the CSI matrix is $8 \times 2 + (3 + 8 \times 2 \times 4 \times 2) \times 52 = 6838$ bits.

Compressed CSI is composed of the SNR and angle information. The SNR is 8 bits per RX antenna. When the transmitter has four antennas and the receiver has two antennas, the angle information is 5 ϕ and 5 ψ. The number of quantization bits of ϕ and ψ differs between the single-user (SU) and multi-user (MU) feedback types. For SU type feedback, the numbers of quantization bits of ϕ and ψ are (4, 2) or (6, 4). From the above conditions, the total data size of compressed CSI is $8 \times 2 + (6 \times 5 + 4 \times 5) \times 52 = 2616$ bits. Thus, compressed CSI compresses the data size to approximately 40 % compared with the original CSI matrix. The importance of compressed CSI will increase with the increase in the number of antennas expected in future wireless communication.

Figure 3 shows simulation results of quantization error. We simulated the effect of quantization error on AoA estimation accuracy. For IEEE 802.11ac, the representation bits of ϕ and ψ are (4,2), (6,4), (7,5), and (9,7) [81]. Note that 802.11ax is able to obtain more detailed information than 802.11n, such as expanding the types of bandwidth and the number of antennas. The quantization error of phase difference between antennas is about 11.3 degrees when the representation bits of ϕ and ψ are (4,2) bits. Similarly, it is about 2.8, 1.4, 0.35 degrees, respectively. The AoA estimation error is almost the same as the above phase difference error. We cannot ignore the effect of quantization error, but its effect is relatively smaller than what this paper will show in Section III.

C. ANTENNA WIRELINE PROBLEM

The phases of CSI observed at the RX antennas should follow Equation (3). However, each phase changes depending on the length of the wireline from each RX antenna to the AD converter. Therefore, $\mathbf{CSI}'_{*,n}$, which reflects the effects of the length of the wireline between the antenna and the AD converter in Equation (3), is determined as:

$$\mathbf{CSI}'_{*,n} = \begin{pmatrix} a_1 e^{j\Theta + j2\pi f \frac{0 \cdot d\sin(\theta)}{c} + j\tau_1} \\ a_2 e^{j\Theta + j2\pi f \frac{1 \cdot d\sin(\theta)}{c} + j\tau_2} \\ \vdots \\ a_M e^{j\Theta + j2\pi f \frac{(M-1) \cdot d\sin(\theta)}{c} + j\tau_M} \end{pmatrix} \tag{9}$$

where τ_m $(m = 1, 2, \ldots, M)$ is the phase change dependent on wireline length.

D. ANTENNA SPACING PROBLEM

When a phase is obtained from a radio wave, the correct value of the phase difference can be obtained only when the distance between the RX antennas is less than or equal to $\lambda/2$ where λ is the wavelength of the radio wave. The range of $\widetilde{h}_i$, which is the phase difference acquired from CSI, is expressed as follows.

$$-\pi < \widetilde{h}_i \leq \pi \tag{10}$$

We can also express $\widetilde{h}_i$ as shown in Equation (11) by combining Equation (1) and Equation (10).

$$-\pi < -2\pi f \frac{d\sin(\theta)}{c} \leq \pi \tag{11}$$

Solving Equation (11) for d yields Equation (12).

$$-\frac{c}{2f\sin(\theta)} < d \leq \frac{c}{2f\sin(\theta)} \tag{12}$$

As $-1 < \sin(\theta) \leq 1$, Equation (12) can be expressed as shown in Equation (13).

$$-\frac{c}{2f} < d \leq \frac{c}{2f} \tag{13}$$

By combining Equation (13), $\lambda = \frac{c}{f}$, and $d > 0$, we obtain Equation (14).

$$0 < d \leq \frac{\lambda}{2} \tag{14}$$

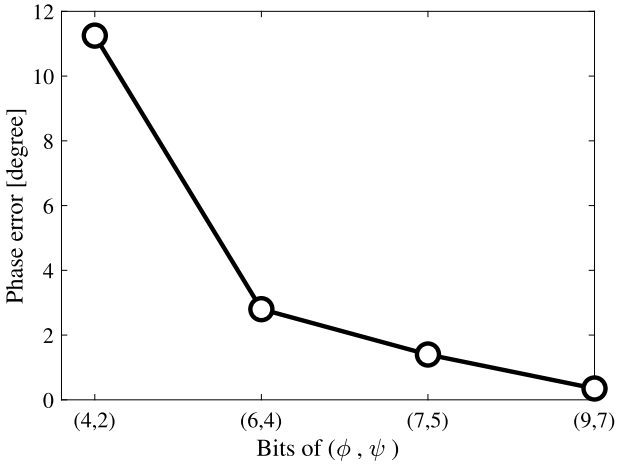

FIGURE 3. Simulation results for quantization error.

FIGURE 4. Example of WLAN access point.

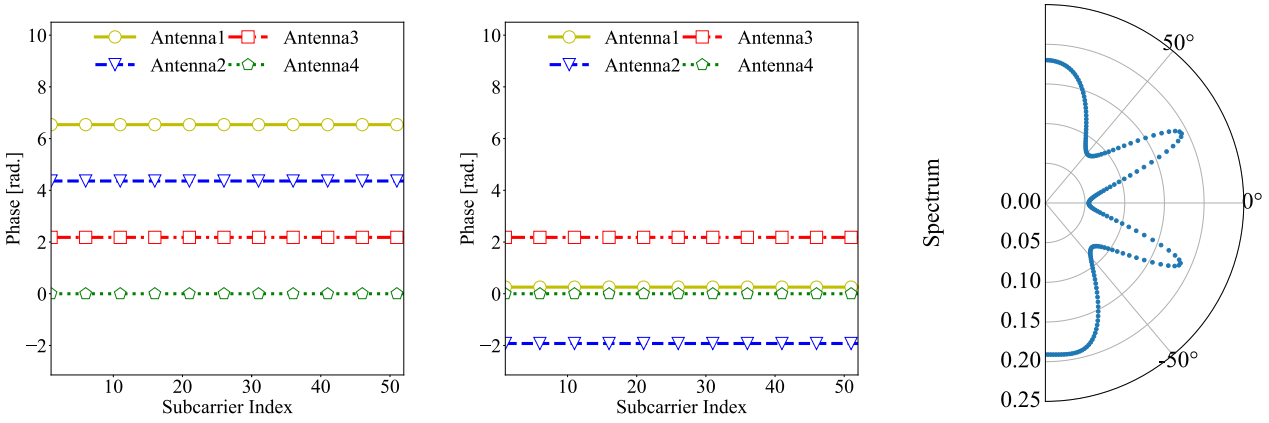

(a) True phase difference

(b) Phase difference calculated from compressed CSI

(c) MUSIC spectrum estimated with truncated phase difference

FIGURE 5. Simulation result of phase difference and MUSIC spectrum when AoA is 30°.

However, the distance between the antennas in commercial WLAN devices is made larger than $\frac{\lambda}{2}$ to lower the spatial correlation and thus improve the MIMO transmission performance. Figure 4 shows an example of an access point. The λ of 5 GHz is approximately 6 cm. The distance between the access point antennas is larger than 3 cm. When the distance between the RX antennas exceeds $\frac{\lambda}{2}$, the phase difference between adjacent antennas sometimes exceeds 360°, and the phase difference is truncated to fit between $-\pi$ and π, making it impossible to estimate AoA correctly.

For example, suppose f is 5.2 GHz, d is 4 cm, and the number of RX antennas is 4. Figure 5(a) shows the correct values of the phase when the AoA is 30° and the phase of Antenna4 is 0 rad. The vertical axis is the phase and the horizontal axis is the subcarrier index. The phase difference is approximately 2.17 rad. If the phase of Antenna4 is 0 rad, the correct phases of Antenna3, Antenna2, and Antenna1 are approximately 2.17, 4.34, and 6.51 rad, respectively. However, as CSI is a complex number, the acquired phase is truncated between $-\pi$ and π. Figure 5(b) shows the phase acquired from CSI. If the phase of Antenna4 is 0 rad, the phase of Antenna3 is approximately 2.17 rad, but the phase of Antenna2 is truncated to approximately -1.92 rad, and the phase of Antenna1 is also truncated to approximately 0.26 rad. Figure 5(c) shows a multiple signal classification (MUSIC) spectrum using the phase of Figure 5(b). A peak appears at 30°, but peaks also appear at 89°, $-30°$, and $-80°$.

E. ANTENNA INDIVIDUALITY PROBLEM

Antenna arrays for AoA estimation such as radars are designed assuming that the receiving conditions of the antennas are as equal as possible. However, because of the requirements of MIMO transmission as described in Section III-D, each RX antenna in actual WLAN devices should be expected to have a different receiver condition. Consequently, the phase acquired by each RX antenna in WLAN devices may be individually affected by housing, circuit boards, and the installation environment. When the AoA is estimated using RX antennas with largely different receiving conditions, the estimated value may be significantly different from the correct value.

IV. AOA ESTIMATION ON IEEE 802.11AC AND IEEE 802.11AX

A. OVERVIEW

To solve the four problems described in Section III, we propose a practical AoA estimation method; this paper focuses on IEEE 802.11ac and IEEE 802.11ax WLAN devices. The proposed method estimates AoA with the following four procedures, which correspond to the four problems described in Section III.

1) Convert the angle information in compressed CSI to the right singular matrix $\mathbf{V}$, which includes the relative phase information among the antennas.
2) Calibrate the right singular matrix $\mathbf{V}$ using $\mathbf{V}$ at 0°, which is expected to be known before factory shipment.
3) Calibrate phases using a brute force algorithm to equalize all the phase differences.
4) Select the optimal combination of antennas with kurtosis and the number of peaks using the MUSIC spectrum.

B. SOLUTION FOR COMPRESSED CSI PROBLEM

To solve the compressed CSI problem described in Section III-B, AoAac/ax restores the relative phase difference information from compressed CSI. Note that proposed method assumes that the distance between the transmitter and the receiver is infinity, and the angles of departure (AoD) and AoA are equal. On the basis of the above assumptions, the proposed method utilizes the right singular matrix $\mathbf{V}$ including the relative phase information of the CSI from the TX antennas to the RX antennas.

First, the proposed method calculates $\mathbf{V}$ through the substitution of ϕ and ψ into Equations (6), (7), and (8). The right singular matrix $\mathbf{V}$ is expressed as follows:

$$\mathbf{V} = \begin{pmatrix} v_{1,1} & v_{1,2} & \cdots & v_{1,M} \\ v_{2,1} & v_{2,2} & \cdots & v_{2,M} \\ \vdots & \ddots & \vdots & \\ v_{N,1} & v_{2,N} & \cdots & v_{N,M} \end{pmatrix} \tag{15}$$

As we assume that AoD is equal to AoA, the column vector of right singular matrix V is regarded as the relative phase difference from N TX antennas to M Rx antennas. To use V for AoA estimation, the proposed method uses $\mathbf{V}_{*,1}$, which is the first column of $\mathbf{V}$ as follows based on Equation (5).

$$\mathbf{V}_{*,1} = \begin{pmatrix} v_{1,1} \\ v_{2,1} \\ \vdots \\ v_{N,1} \end{pmatrix} = \begin{pmatrix} A_1 e^{j2\pi f_l \frac{(N-1)\cdot d\sin(\theta)}{c}} \\ A_2 e^{j2\pi f_l \frac{(N-2)\cdot d\sin(\theta)}{c}} \\ \vdots \\ A_N e^{j2\pi f_l \frac{0\cdot d\sin(\theta)}{c}} \end{pmatrix} \tag{16}$$

where A_n $(n = 1, \ldots, N)$ is the amplitude of each element of V. The proposed method extracts $h_{\mathrm{V},i}$, which is the phase difference between TX antenna 1 and i $(i = 2, 3, \cdots, N)$, using Equation (16) as follows:

$$h_{\mathrm{V},i} = \frac{v_{i,1}}{v_{1,1}} \tag{17}$$

C. SOLUTION FOR ANTENNA WIRELINE PROBLEM

To solve the antenna wireline problem described in Section III-C, the proposed method calibrates the right singular matrix $\mathbf{V}$ using the offset acquired by $\mathbf{V}$ at 0° before factory shipment. The calibration involves four steps:

1) Acquire the right singular matrix $\hat{\mathbf{V}}$ when the AoA is 0° before factory shipment.
2) Extract the phase from matrix $\hat{\mathbf{V}}$.
3) Use the extracted phase to calculate phase offset τ_N with the average of the phase at each subcarrier.
4) Calibrate the right singular matrix $\mathbf{V}$ using τ_N during actual AoA estimation.

Before factory shipment, the proposed method acquires a singular matrix $\hat{\mathbf{V}}$ when the AoA is 0°, and $\hat{\mathbf{V}}_{*,1}$ is formulated as follows:

$$\hat{\mathbf{V}}_{*,1} = \begin{pmatrix} \hat{v}_{1,1} \\ \hat{v}_{2,1} \\ \vdots \\ \hat{v}_{N,1} \end{pmatrix} = \begin{pmatrix} \hat{A}_1 e^{j\tau_{N,l}} \\ \hat{A}_2 e^{j\tau_{N-1,l}} \\ \vdots \\ \hat{A}_N e^{j\tau_{1,l}} \\ \cdot \end{pmatrix} \tag{18}$$

The proposed method calculates τ_m as follows:

$$\tau_i = \arg\left(\frac{\hat{v}_{i,1}}{\hat{v}_{1,1}}\right) \tag{19}$$

Using Equations (19) and (17), $h_{0\mathrm{DC},i}$, which is the calibrated phase difference, is formulated as follows.

$$h_{0\mathrm{DC},i} = h_{\mathrm{V},i} + \tau_i \tag{20}$$

D. SOLUTION FOR ANTENNA SPACING PROBLEM

To solve the antenna spacing problem described in Section III-D, the proposed method performs phase restoration and frequency adjustment as follows.

E. PHASE RESTORATION

When $d > \frac{\lambda}{2}$, the phase restoration is performed using Equation (21).

$$h_{\mathrm{PR},i} = h_{0\mathrm{DC},i} - h_{0\mathrm{DC},1} + 2\pi r_i \tag{21}$$

where $h_{\mathrm{PR},i}$ is the phase after restoration, $h_{0\mathrm{DC},i}$ is the phase before restoration, and r_i is the number of phase rotations. $h_{\mathrm{PR},i}$ is the correct phase difference including the phase rotation between RX antenna 1 and RX antenna i when $h_{0\mathrm{DC},i}$ is extracted as described in Sections IV-B and IV-C. Note that r_i is an unknown number. From Equation (1), the relationship between h_{i+1} and h_i is expressed by Equation (22).

$$h_{\mathrm{PR},i+1} = h_{\mathrm{PR},i} + 2\pi f \frac{d\sin(\theta)}{c} \tag{22}$$

When all the distances between adjacent antennas are equal, we obtain Equation (23) using Equation (21) and Equation (22).

$$\begin{aligned} r_1, r_2, \cdots, r_N = \underset{r_1, r_2, \cdots, r_N}{\arg\min} & \sum_{i=1}^{N-2} (h_{\mathrm{PR},i+2} - h_{\mathrm{PR},i+1}) \\ & (h_{\mathrm{PR},i+1} - h_{\mathrm{PR},i}) \\ & \text{s.t. } 0 \le |r_1| \le |r_2| \le \cdots \le |r_N| \le |r_{\max}| \end{aligned} \tag{23}$$

where $r_{\max}$ is the maximum number of phase rotations.

$r_{\max}$ is calculated with the non-truncated and maximum phase difference between antenna 1 and antenna N. The non-truncated phase difference between TX antenna 1 and TX antenna N is given by Equation (24).

$$h_{\mathrm{PR},N} = 2\pi f \frac{(N-1)d\sin(\theta)}{c} \tag{24}$$

Combining Equations (10), (21), and (24) yields Equation (25).

$$-\pi < 2\pi f \frac{(N-1)d\sin(\theta)}{c} - 2\pi r_N \le \pi \tag{25}$$

Solving Equation (25) for r_N yields Equation (26).

$$f\frac{(N-1)d\sin(\theta)}{c} - \frac{1}{2} \le r_N < f\frac{(N-1)d\sin(\theta)}{c} + \frac{1}{2} \tag{26}$$

When θ is 90°, r_N is equal to $r_{\max}$. Therefore, Equation (26) is expressed as Equation (27).

$$0 \le f\frac{(N-1)d}{c} - \frac{1}{2} \le r_{\max} < f\frac{(N-1)d}{c} + \frac{1}{2} \tag{27}$$

As $r_{\max}$ is an integer, we obtain Equation (28).

$$r_{\max} = \left\lceil f\frac{(N-1)d}{c} - \frac{1}{2} \right\rceil \tag{28}$$

where $\left\lceil f\frac{(N-1)d}{c} - \frac{1}{2} \right\rceil$ represents the least integer greater than or equal to $f\frac{(N-1)d}{c} - \frac{1}{2}$.

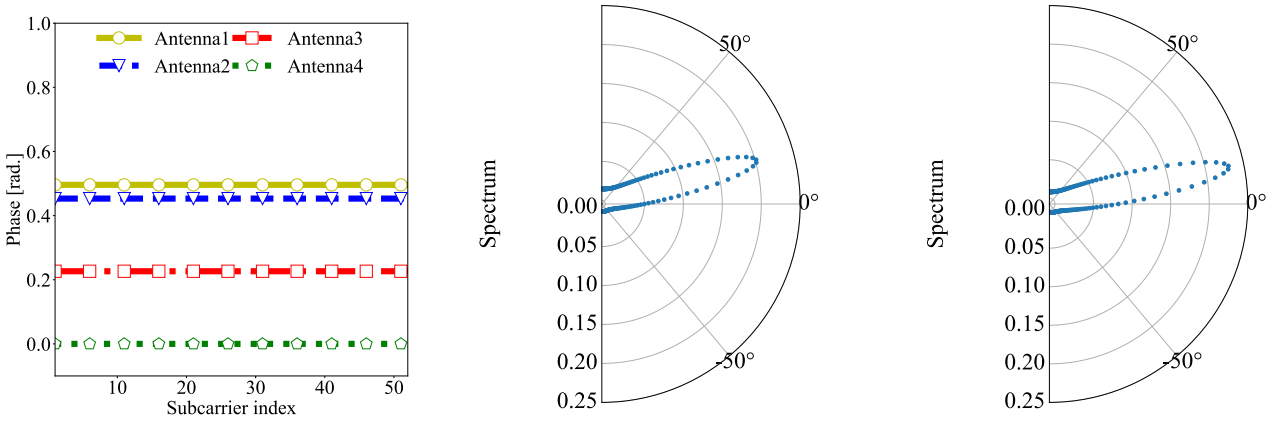

(a) Phase extracted from $\mathbf{V}$

(b) Spectrum using all phases
Estimated AoA $= 16°$
Kurtosis $= 3.8$

(c) Spectrum using phase of Antenna3 and Antenna4
Estimated AoA $= 12°$
Kurtosis $= 4.4$

FIGURE 6. Acquired phase and estimated spectrum when AoA is 10°.

F. FREQUENCY ADJUSTMENT

Even if the phase restoration is performed as described above before AoA estimation, MUSIC treats the phase difference internally as a complex number and truncates the phase difference between $-\pi$ and π again. To solve the re-truncation problem, the proposed method adjusts the frequency so that $r_{\max} = 0$ using Equation (29).

$$h_{\mathrm{FA},i} = \frac{f_{\mathrm{adjust}}}{f_{\mathrm{raw}}} h_{\mathrm{PR},i} \tag{29}$$

where $h_{\mathrm{FA},i}$ is the adjusted phase, $h_{\mathrm{PR},i}$ is the phase restored using Equation (21), f_{raw} is the frequency at which the compressed CSI is sent, and f_{adjust} is the frequency to adjust the phase in order to truncate the phase difference between $-\pi$ and π. By combining $r_{\max} = 0$ and Equation (28), f_{adjust} is calculated using Equation (30).

$$f_{\mathrm{adjust}} = \frac{c}{2(N-1)d} \tag{30}$$

G. SOLUTION FOR ANTENNA INDIVIDUALITY PROBLEM

To solve the antenna individuality problem described in Section III-E, the proposed method runs a heuristic algorithm to select the combination of antennas that achieves precise AoA estimation. Algorithm 1 shows the proposed antenna selection algorithm. $\mathbb{H}$ is a set of calibrated phases as described in Section IV-D, N is the number of TX antennas, s ($\in$ $\mathbb{S}$) is the MUSIC spectrum, and $\hat{s}$ is the spectrum yielded by the best antenna combination. The function "combinations($\mathbb{H}$, i)" returns a set of combinations of i phases from $\mathbb{H}$, and it corresponds to nchoosek() in MATLAB and itertools.combination() in Python. The function "findpeaks(s)" returns the number of peaks in MUSIC spectrum s and corresponds to findpeaks() in MATLAB and scipy.signal.argrelmax() in Python. The function "kurtosis(s)" returns the kurtosis of MUSIC spectrum s and corresponds to kurtosis() in MATLAB and scipy.stats.kurtosis() in Python. First, Algorithm 1 uses the number of peaks in the MUSIC spectrum for the antenna selection. The presence of multiple peaks indicates that the AoA estimation error is large. When there is only one peak in the MUSIC spectrum, Algorithm 1 uses the kurtosis of the MUSIC spectrum for antenna selection.

Figure 6 shows an example of antenna selection. Figure 6(a) is the observed phase of the right singular matrix $\mathbf{V}$ for an AoA of 10°. AoA estimation using the phases of Antenna3 and Antenna4 is more accurate than that gained by using the phases of four antennas. Figure 6(b) is the MUSIC spectrum estimated using the phase of all antennas, and Figure 6(c) is the MUSIC spectrum estimated using the phase of four antennas. The kurtosis of the spectrum in Figure 6(b) and Figure 6(c) is approximately 3.8 and 4.4, respectively.

V. EVALUATION

A. EVALUATION SETTINGS

Figures 7, 8, 9, and 10 show the evaluation environments: a lecture room and a shield tent. AP in Figure 7 and Figure 9 represents an access point, and PC represents a user device. In the shield tent, the access point and user device were surrounded by radio wave absorbers. The distance between the access point and the user device was 2.5 m. The access point was an NTT EA-7HW04AP1ES, which supports IEEE 802.11ac, and the user device was a Panasonic Let's note CF-SZ6. There were no obstacles between the access point and the user device.

Table 1 shows the evaluation parameters. The radio frequency was 5.2 GHz, the number of antennas at the access point was 4, the antenna spacing of the access point was 4 cm, the number of user device antennas was 2, and the antenna spacing of the user device was 36.0 cm. The evaluated

Algorithm 1 Antenna Selection Algorithm

$\mathbb{H} = \{h_{\mathrm{PR},1}, h_{\mathrm{PR},2}, \cdots, h_{\mathrm{PR},N}\}$
$N \leftarrow$ the number of TX antennas
$\mathbb{S} \leftarrow \emptyset$
$p_{\min} \leftarrow \infty$
$k_{\max} \leftarrow -\infty$
for $i = 1, 2, \cdots, N$ **do**
  $\mathbb{C} = \mathrm{combinations}(\mathbb{H}, i)$
  for each $H_{\mathrm{selected}} \in \mathbb{C}$ **do**
    $s = \mathrm{music}(H_{\mathrm{selected}})$
    $\mathbb{S} \leftarrow \mathbb{S} \cup \{s\}$
  end for each
end for
for each $s \in \mathbb{S}$ **do**
  if $p = \mathrm{findpeaks}(s) \leq p_{\min}$ **then**
    $p_{\min} = p$
    if $k = \mathrm{kurtosis}(s) > k_{\max}$ **then**
      $k_{\max} = k$
      $\hat{s} = s$
    end if
  end if
end for each
return $\hat{s}$

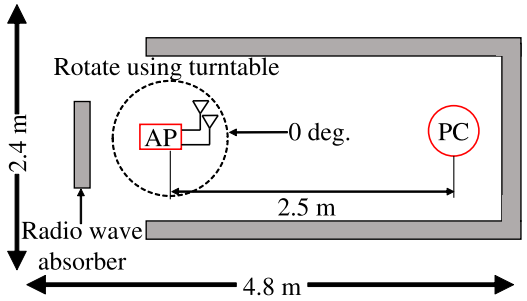

FIGURE 7. Layout in shield tent.

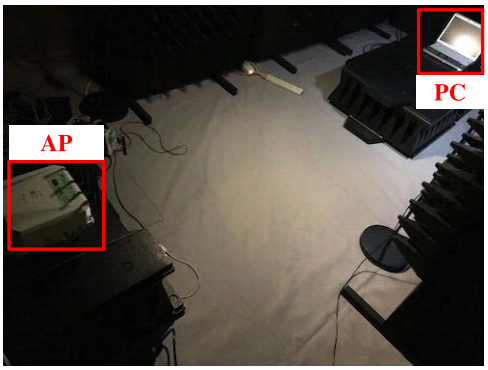

FIGURE 8. Photograph of shield tent.

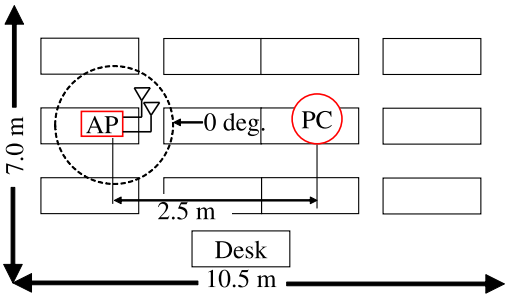

FIGURE 9. Layout in lecture room.

TABLE 1. Evaluation parameters.

Frequency	5.2 GHz
Antenna distance of access point	4.0 cm
Antenna distance of user device	36.0 cm
Number of trials	100
Number of access point antennas	4
Number of user device antennas	2
Number of subcarriers	52
Evaluated AoA range	from $-80°$ to $80°$

AoA was varied from $-80°$ to $80°$ in steps of $10°$ using a turntable. The number of trials of AoA estimation at each AoA was 100. We used 52 subcarriers and the general MUSIC algorithm to calculate the MUSIC spectrum.

To evaluate the effect of each solution presented in Section IV for the proposed method, we implemented and evaluated four methods using Python:

1) V: AoA estimation using the MUSIC algorithm and the right singular matrix $\mathbf{V}$ restored from the compressed CSI described in Section IV-B.
2) V+0DC: AoA estimation adding $0°$ calibration (0DC), which is described in Section IV-C, to the above V. 0DC is a phase calibration method.
3) V+0DC+PRFA: AoA estimation adding phase restoration and frequency adjustment (PRFA), which are described in Section IV-D, to the above V+0DC.
4) Proposed: This is the proposed approach. AoA estimation adding antenna selection (AS), which is described in Section IV-G, to the above V+0DC+PRFA.

AoA was estimated on a MacBook Pro Mid 2017 (MPXT2J/A).

B. ACCURACY

Figures 11 and 12 show the average AoA estimation errors in the shield tent and lecture room, respectively. The vertical axis is the average AoA estimation error at each angle, and the horizontal axis is the ground truth of the AoA.

In the shield tent, the average AoA estimation errors at all angles of V, V+0DC, V+0DC+PRFA, and the proposed method were approximately $53.8°$, $62.0°$, $14.4°$, and $9.1°$, respectively. In the lecture room, the average AoA estimation errors at all angles of V, V+0DC, V+0DC+PRFA,

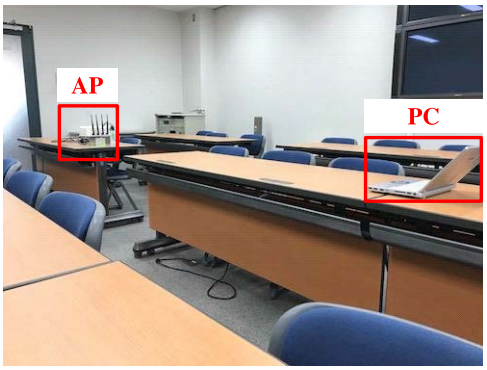

FIGURE 10. Photograph of lecture room.

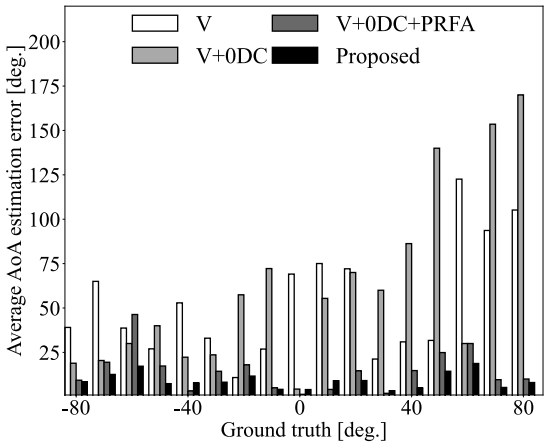

FIGURE 11. Average AoA estimation error in shield tent.

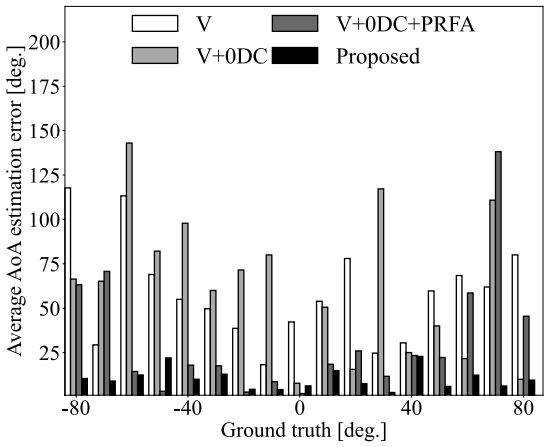

FIGURE 12. Average AoA estimation error in lecture room.

and the proposed method were approximately 58.36°, 62.6°, 32.0°, and 10.18°, respectively. From the average AoA estimation error in the two environments, we can observe that the proposed method achieved the highest accuracy. Additionally, the AoA estimation in the shield tent was more accurate than that in the lecture room. The evaluation results include those obtained in different environment results such as when AP was rotated from −80° to 80°. The proposed method remained effective for AoA estimation even in actual environments or AP was rotated. However, at some angles, V+0DC+PRFA was more accurate than the proposed method. For example, at −40° in the lecture room, the proposed method had an average error of approximately 7.8°, whereas V+0DC+PRFA had an average error of approximately 3.3°.

Figures 13 and 14 show the average variances of the estimated AoA in the shield tent and lecture room, respectively. The vertical axis is the average variance of AoA estimation at each angle, and the horizontal axis is the ground truth of the AoA.

In the shield tent, the average variances at all angles of V, V+0DC, V+0DC+PRFA, and the proposed method were approximately 668.95, 109.25, 4.40, and 1.90, respectively. In the lecture room, the average variances at all angles of V, V+0DC, V+0DC+PRFA, and the proposed method were approximately 612.52, 598.59, 331.39, and 33.42, respectively. The proposed method achieved the smallest variance among the four AoA estimation methods. Additionally, AoA estimation in the shield tent had a lower variance than that in the lecture room. Furthermore, there was no correlation between the average AoA estimation error and the average variance of the estimated AoA. For example, the average AoA estimation error of the proposed method in the lecture room at −20° was approximately 4.94°, but the variance of the proposed method in the lecture room at −20° was approximately 193.7. In contrast, the average AoA estimation error of the proposed method in the lecture room at 10° was approximately 9.1°, but the variance of the proposed method in the lecture room at 10° was approximately 0.2. We believe that the proposed method yielded an error offset for some unknown reason. We think that the antenna directional and the antenna accuracy of the devices may have affected the AoA estimation error.

Then, we evaluated the existing AoA estimation in the same environment. Figure 15 shows the cumulative frequency (CDF) of the proposed method and SpotFi [15]. The vertical axis is the CDF, and the horizontal axis is the AoA estimation error. The median AoA estimation errors of the proposed method in shield tent and lecture room were 7.0° and 7.2°, respectively. The median AoA estimation errors of SpotFi in the shield tent and lecture room were 40.5° and 42.0°, respectively. From Figure 15, the previous AoA estimation methods cannot solve the problems described in Section III, while the proposed method can.

C. COMPUTATION TIME

Figure 16 and Figure 17 show the computation times of AoA estimation in the shield tent and lecture room, respectively. The vertical axis is the computation time for AoA estimation, and the horizontal axis is the AoA ground truth. From the

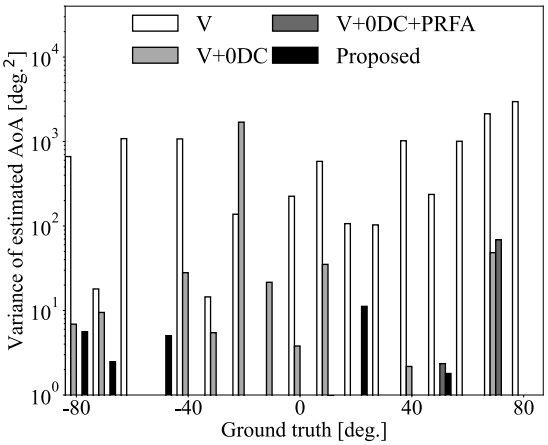

FIGURE 13. Variance of AoA estimation error in shield tent.

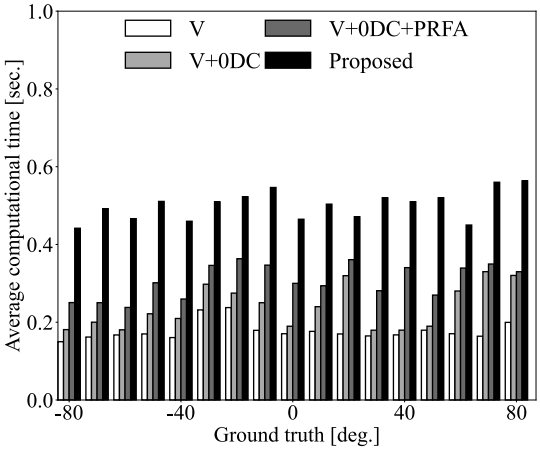

FIGURE 16. Computation time in shield tent.

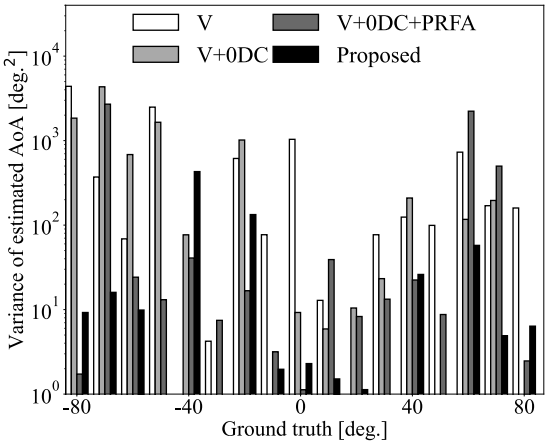

FIGURE 14. Variance of AoA estimation error in lecture room.

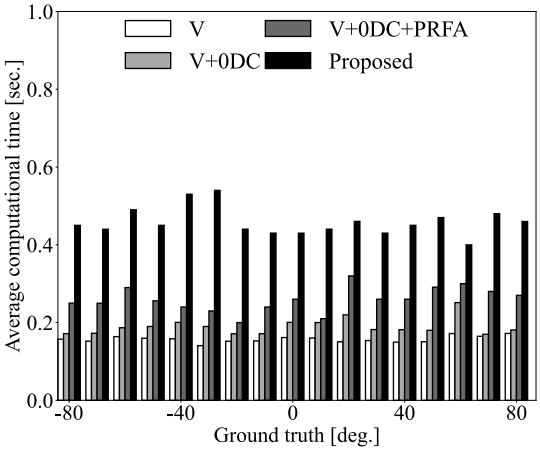

FIGURE 17. Computation time in lecture room.

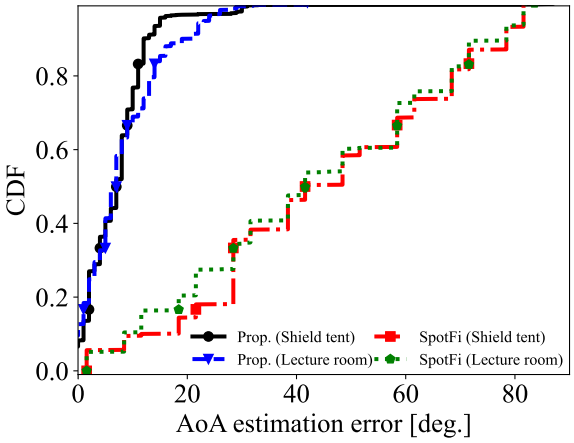

FIGURE 15. Comparison of AoA estimation.

figures, we can observe that V, V+0DC, V+0DC+PRFA, and the proposed method calculated the AoA within 1 s, regardless of the AoA ground truth. The average computation times at all angles of V, V+0DC, V+0DC+PRFA, and the proposed method in the shield tent were approximately 0.18, 0.24, 0.31, and 0.50 s, respectively. The average computation times at all angles of V, V+0DC, V+0DC+PRFA, and the proposed method in the lecture room were approximately 0.16, 0.19, 0.26, and 0.46 s, respectively. Additionally, the highest computation cost was observed for the antenna selection algorithm described in Section IV-G. Furthermore, the computation time of MUSIC was neither short nor stable and depends on the propagation path.

VI. CONCLUSION

We proposed a practical method for successfully estimating AoA from the compressed CSI specified by IEEE 802.11ac and IEEE 802.11ax. The proposed method advances the current research toward wide deployment because it can estimate AoA using commercially available IEEE 802.11ac and IEEE 802.11ax WLAN devices without CSI tools such as the Atheros CSI tool, Intel 5300 NIC, or Atheros 802.11n

chipsets. This method solves four problems with AoA estimation using compressed CSI and estimates AoA with an average error of 9.1°. The results of this study not only indicate that we could estimate AoA from compressed CSI but also the possibility of expanding current CSI-tool-based wireless sensing into wide deployment. We believe that the use of compressed CSI will contribute to a future where deploying WLAN access points means making a platform that provides both communication and sensing. Our future work will exploit the channel-state information of multiple links and multiple antennas to improve the AoA estimation accuracy.

REFERENCES

[1] X. Cui, T. A. Gulliver, J. Li, and H. Zhang, "Vehicle positioning using 5G millimeter-wave systems," *IEEE Access*, vol. 4, pp. 6964–6973, 2016.

[2] S. Jung, S. Hwang, H. Shin, and D. H. Shim, "Perception, guidance, and navigation for indoor autonomous drone racing using deep learning," *IEEE Robot. Autom. Lett.*, vol. 3, no. 3, pp. 2539–2544, Jul. 2018.

[3] S. Sen, D. Kim, S. Laroche, K.-H. Kim, and J. Lee, "Bringing CUPID indoor positioning system to practice," in *Proc. 24th Int. Conf. World Wide Web*, May 2015, pp. 938–948.

[4] B. Kempke, P. Pannuto, and P. Dutta, "PolyPoint: Guiding indoor quadrotors with ultra-wideband localization," in *Proc. 2nd Int. Workshop Hot Topics Wireless*, Sep. 2015, pp. 16–20.

[5] F. Reclus and K. Drouard, "Geofencing for fleet & freight management," in *Proc. 9th Int. Conf. Intell. Transp. Syst. Telecommun., (ITST)*, Oct. 2009, pp. 353–356.

[6] D. Namiot and M. S. Sneppe, "Geofence and network proximity," in *Internet Things, Smart Spaces, Next Generation Networking* (Lecture Notes in Computer Science), vol. 8121. Cham, Switzerland: Springer, 2013, pp. 117–127.

[7] D. Chen, K. G. Shin, Y. Jiang, and K.-H. Kim, "Locating and tracking BLE beacons with smartphones," in *Proc. 13th Int. Conf. Emerg. Netw. EXperiments Technol.*, Nov. 2017, pp. 263–275.

[8] Z. Fu, J. Xu, Z. Zhu, A. X. Liu, and X. Sun, "Writing in the air with WiFi signals for virtual reality devices," *IEEE Trans. Mobile Comput.*, vol. 18, no. 2, pp. 473–484, Feb. 2019.

[9] M. Kotaru and S. Katti, "Position tracking for virtual reality using commodity WiFi," in *Proc. IEEE Conf. Comput. Vis. Pattern Recognit. (CVPR)*, Jul. 2017, pp. 68–79.

[10] K. Witrisal, P. Meissner, E. Leitinger, Y. Shen, C. Gustafson, F. Tufvesson, K. Haneda, D. Dardari, A. F. Molisch, A. Conti, and M. Z. Win, "High-accuracy localization for assisted living: 5G systems will turn multipath channels from foe to friend," *IEEE Signal Process. Mag.*, vol. 33, no. 2, pp. 59–70, Mar. 2016.

[11] M. S. Grewal, L. R. Weill, and A. P. Andrews, *Global Positioning Systems, Inertial Navigation, and Integration*. Hoboken, NJ, USA: Wiley, 2007.

[12] J. Xiong and K. Jamieson, "ArrayTrack: A fine-grained indoor location system," in *Proc. USENIX Symp. (NSDI)*. Chicago, IL, USA, Apr. 2013, pp. 71–84.

[13] S. Jeong, O. Simeone, and J. Kang, "Optimization of massive full-dimensional MIMO for positioning and communication," *IEEE Trans. Wireless Commun.*, vol. 17, no. 9, pp. 6205–6217, Sep. 2018.

[14] S. Kumar, S. Gil, D. Katabi, and D. Rus, "Accurate indoor localization with zero start-up cost," in *Proc. 20th Annu. Int. Conf. Mobile Comput.*, Sep. 2014, pp. 483–494.

[15] M. Kotaru, K. Joshi, D. Bharadia, and S. Katti, "SpotFi: Decimeter level localization using WiFi," in *Proc. ACM SIGCOMM*, London, U.K., Aug. 2015, pp. 269–282.

[16] X. Xiong, K. Sundaresan, and K. Jamieson, "ToneTrack: Leveraging frequency-agile radios for time-based indoor wireless localization," in *Proc. 21st Annu. Intl. Conf. Mobile Comput. Netw. (MobiCom)*, Sep. 2015, pp. 537–549.

[17] D. Vasisht, S. Kumar, and D. Katabi, "Decimeter-level localization with a single WiFi access point," in *Proc. 13th USENIX Symp. Netw. Syst. Design Implement. (NSDI)*, Mar. 2016, pp. 165–178.

[18] E. Soltanaghaei, A. Kalyanaraman, and K. Whitehouse, "Multipath triangulation: Decimeter-level WiFi localization and orientation with a single unaided receiver," in *Proc. 16th Annu. Int. Conf. Mobile Syst., Appl., Services*, Jun. 2018, pp. 376–388.

[19] T.-C. Tai, K. C.-J. Lin, and Y.-C. Tseng, "Toward reliable localization by unequal AoA tracking," in *Proc. 17th Annu. Int. Conf. Mobile Syst., Appl., Services*, Jun. 2019, pp. 444–456.

[20] R. Ayyalasomayajula, A. Arun, C. Wu, S. Rajagopalan, S. Ganesaraman, A. Seetharaman, I. K. Jain, and D. Bharadia, "LocAP: Autonomous millimeter accurate mapping of WiFi infrastructure," in *Proc. 17th USENIX Symp. Netw. Syst. Design Implement.*, Feb. 2020, pp. 1115–1129.

[21] Y. Ma, X. Hui, and E. C. Kan, "3D real-time indoor localization via broadband nonlinear backscatter in passive devices with centimeter precision," in *Proc. 22nd Annu. Int. Conf. Mobile Comput. Netw.*, New York, NY, USA, Oct. 2016, pp. 216–229.

[22] Y. Ma, N. Selby, and F. Adib, "Minding the billions: Ultra-wideband localization for deployed RFID tags," in *Proc. 23rd Annu. Int. Conf. Mobile Comput. Netw.*, Snowbird, UT, USA, Oct. 2017, pp. 248–260.

[23] M. B. Akbar, D. G. Taylor, and G. D. Durgin, "Hybrid inertial microwave reflectometry for mm-scale tracking in RFID systems," *IEEE Trans. Wireless Commun.*, vol. 14, no. 12, pp. 6805–6814, Dec. 2015.

[24] N. Xiao, P. Yang, X. Li, Y. Zhang, Y. Yan, and H. Zhou, "MilliBack: Real-time plug-n-play millimeter level tracking using wireless backscattering," in *Proc. ACM Interact., Mobile, Wearable Ubiquitous Technol.*, Sep. 2019, pp. 112:1–112:23.

[25] Y. Wang, X. Yang, Y. Zhao, Y. Liu, and L. Cuthbert, "Bluetooth positioning using RSSI and triangulation methods," in *Proc. IEEE Consum. Commun. Netw. Conf. (CCNC)*, Jan. 2013, pp. 837–842.

[26] X. Tong, K. Liu, X. Tian, L. Fu, and X. Wang, "FineLoc: A fine-grained self-calibrating wireless indoor localization system," *IEEE Trans. Mobile Comput.*, vol. 18, no. 9, pp. 2077–2090, Sep. 2019.

[27] A. Coliccia, "Reduced-bias ML-based estimators with low complexity for self-calibrating RSS ranging," *IEEE Trans. Wireless Commun.*, vol. 12, no. 3, pp. 1220–1230, Mar. 2013.

[28] Y. Chen, J. Yang, W. Trappe, and R. P. Martin, "Detecting and localizing identity-based attacks in wireless and sensor networks," *IEEE Trans. Veh. Technol.*, vol. 59, no. 5, pp. 2418–2434, Mar. 2010.

[29] M. R. Basheer and S. Jagannathan, "Localization and tracking of objects using cross-correlation of shadow fading noise," *IEEE Trans. Mobile Comput.*, vol. 13, no. 10, pp. 2293–2305, Oct. 2014.

[30] J. Palacios, G. Bielsa, P. Casari, and J. Widmer, "Single- and multiple-access point indoor localization for millimeter-wave networks," *IEEE Trans. Wireless Commun.*, vol. 18, no. 3, pp. 1927–1942, Mar. 2019.

[31] J. Naganawa, H. Miyazaki, and H. Tajima, "Localization accuracy model incorporating signal detection performance for wide area multilateration," *IEEE Trans. Aerosp. Electron. Syst.*, vol. 55, no. 4, pp. 1957–1971, Aug. 2019.

[32] L. Taponecco, A. A. D'Amico, and U. Mengali, "Joint TOA and AOA estimation for UWB localization applications," *IEEE Trans. Wireless Commun.*, vol. 10, no. 7, pp. 2207–2217, Jul. 2011.

[33] S. Zhang, W. Wang, S. Tang, S. Jin, and T. Jiang, "Robot-assisted backscatter localization for IoT applications," *IEEE Trans. Wireless Commun.*, vol. 19, no. 9, pp. 5807–5818, Sep. 2020.

[34] A. Khattab, J. Camp, C. Hunter, P. Murphy, A. Sabharwal, and E. W. Knightly, "WARP: A flexible platform for clean-slate wireless medium access protocol design," *ACM SIGMOBILE Mobile Comput. Commun. Rev.*, vol. 12, no. 1, pp. 56–58, Jan. 2008.

[35] E. Perahia and R. Stacey, *Next Generation Wireless LANs: 802.11n and 802.11ac*. Cambridge, U.K.: Cambridge Univ. Press, 2013.

[36] D. Halperin, W. Hu, A. Sheth, and D. Wetherall. *Linux 802.11n CSI Tool*. Accessed: Jan. 15, 2020. [Online]. Available: https://dhalperi.github.io/linux-80211n-csitool/

[37] D. Halperin, W. Hu, A. Sheth, and D. Wetherall, "Tool release: Gathering 802.11n traces with channel state information," *ACM SIGCOMM Comput. Commun. Rev.*, vol. 41, no. 1, p. 53, Jan. 2011.

[38] K. Zheng, H. Wang, H. Li, W. Xiang, L. Lei, J. Qiao, and X. S. Shen, "Energy-efficient localization and tracking of mobile devices in wireless sensor networks," *IEEE Trans. Veh. Technol.*, vol. 66, no. 3, pp. 2714–2726, Mar. 2017.

[39] M. Khaledi, M. Khaledi, S. Sarkar, S. Kasera, N. Patwari, K. Derr, and S. Ramirez, "Simultaneous power-based localization of transmitters for crowdsourced spectrum monitoring," in *Proc. 23rd Annu. Int. Conf. Mobile Comput. Netw.*, Oct. 2017, pp. 235–247.

[40] F. Adib, Z. Kabelac, D. Katabi, and R. C. Miller, "3D tracking via body radio reflections," in *Proc. 11th USENIX Conf. Netw. Syst. Design Implement.*, Seattle, WA, USA, Apr. 2014, pp. 317–329.
[41] F. Adib, Z. Kabelac, and D. Katabi, "Multi-person localization via RF body reflections," in *Proc. NSDI*, May 2015, pp. 279–292.
[42] L. Zhang, Q. Gao, X. Ma, J. Wang, T. Yang, and H. Wang, "DeFi: Robust training-free device-free wireless localization with WiFi," *IEEE Trans. Veh. Technol.*, vol. 67, no. 9, pp. 8822–8831, Sep. 2018.
[43] T. J. Pierson, T. Peters, R. Peterson, and D. Kotz, "Proximity detection with single-antenna IoT devices," in *Proc. 25th Annu. Int. Conf. Mobile Comput. Netw.*, Aug. 2019, p. 21.
[44] M. Zhao, F. Adib, and D. Katabi, "Emotion recognition using wireless signals," *Commun. ACM*, vol. 61, no. 9, pp. 91–100, Aug. 2018.
[45] Q. Pu, S. Gupta, S. Gollakota, and S. Patel, "Whole-home gesture recognition using wireless signals," in *Proc. ACM MobiCom*, Sep. 2013, pp. 27–38.
[46] S. Hantscher, B. Schlenther, M. Hagelen, S. A. Lang, H. Essen, A. Tessmann, A. Hulsmann, A. Leuther, and M. Schlechtweg, "Security pre-screening of moving persons using a rotating multichannel W-band radar," *IEEE Trans. Microw. Theory Techn.*, vol. 60, no. 3, pp. 870–880, Mar. 2012.
[47] F. Adib and D. Katabi, "See through walls with Wi-Fi!" in *Proc. Conf. ACM Special Interest Group Data Commun. (ACM SIGCOMM)*, Aug. 2013, pp. 75–86.
[48] F. Adib, C.-Y. Hsu, H. Mao, D. Katabi, and F. Durand, "Capturing the human figure through a wall," *ACM Trans. Graph.*, vol. 34, no. 6, p. 219, Oct. 2015.
[49] L. Yang, Q. Lin, X. Li, T. Liu, and Y. Liu, "See through walls with COTS RFID system!" in *Proc. 21st Annu. Int. Conf. Mobile Comput. Netw.*, Sep. 2015, pp. 487–499.
[50] D. Vasisht, G. Zhang, O. Abari, H.-M. Lu, J. Flanz, and D. Katabi, "In-body backscatter communication and localization," in *Proc. Conf. ACM Special Interest Group Data Commun.*, New York, NY, USA, Aug. 2018, pp. 132–146.
[51] F. Adib, H. Mao, Z. Kabelac, D. Katabi, and R. C. Miller, "Smart homes that monitor breathing and heart rate," in *Proc. ACM CHI*, Seoul South Korea, Apr. 2015, pp. 837–846.
[52] P. Hillyard, A. Luong, A. S. Abrar, N. Patwari, K. Sundar, R. Farney, J. Burch, C. Porucznik, and S. H. Pollard, "Experience: Cross-technology radio respiratory monitoring performance study," in *Proc. 24th Annu. Int. Conf. Mobile Comput. Netw.*, Oct. 2018, pp. 487–496.
[53] X. Zhuge and A. G. Yarovoy, "A sparse aperture MIMO-SAR-based UWB imaging system for concealed weapon detection," *IEEE Trans. Geosci. Remote Sens.*, vol. 49, no. 1, pp. 509–518, Jan. 2011.
[54] J. D. Krieger, Y. Kochman, and G. W. Wornell, "Multi-coset sparse imaging arrays," *IEEE Trans. Antennas Propag.*, vol. 62, no. 4, pp. 1701–1715, Apr. 2014.
[55] C. Gao, Y. Li, and X. Zhang, "LiveTag: Sensing human-object interaction through passive chipless WiFi tags," in *Proc. USENIX Netw. Syst. Design Implement.*, Renton, WA, USA, Apr. 2018, pp. 533–546.
[56] W. Wang, A. X. Liu, M. Shahzad, K. Ling, and S. Lu, "Understanding and modeling of WiFi signal based human activity recognition," in *Proc. ACM MobiCom*, Sep. 2015, pp. 65–76.
[57] W. Jiang, C. Miao, F. Ma, S. Yao, and Y. Wang, "Towards environment independent device free human activity recognition," in *Proc. MobiCom*, New Delhi, India, Oct. 2018, pp. 289–304.
[58] K. Ohara, T. Maekawa, Y. Kishino, Y. Shirai, and F. Naya, "Transferring positioning model for device-free passive indoor localization," in *Proc. ACM Int. Joint Conf. Pervasive Ubiquitous Comput. (UbiComp)*, Osaka, Japan, Sep. 2015, pp. 885–896.
[59] J. Wang, H. Jiang, J. Xiong, K. Jamieson, X. Chen, D. Fang, and B. Xie, "LiFS: Low human-effort, device-free localization with fine-grained subcarrier information," in *Proc. 22nd Annu. Int. Conf. Mobile Comput. Netw.*, Oct. 2016, pp. 243–256.
[60] Y. Xie, J. Xiong, M. Li, and K. Jamieson, "MD-track: Leveraging multi-dimensionality for passive indoor Wi-Fi tracking," in *Proc. 25th Annu. Int. Conf. Mobile Comput. Netw.*, Aug. 2019, pp. 8:1–8:16.
[61] K. Joshi, D. Bharadia, M. Kotaru, and S. Katti, "WiDeo: Fine-grained device-free motion tracing using RF backscatter," in *Proc. USENIX Symp. (NSDI)*. Oakland, CA, USA, May 2015, pp. 189–204.
[62] L. Sun, S. Sen, D. Koutsonikolas, and K.-H. Kim, "WiDraw: Enabling hands-free drawing in the air on commodity WiFi devices," in *Proc. 21st Annu. Int. Conf. Mobile Comput. Netw.*, New York, NY, USA, Sep. 2015, pp. 77–89.
[63] B. Sheng, Y. Fang, F. Xiao, and L. Sun, "An accurate device-free action recognition system using two-stream network," *IEEE Trans. Veh. Technol.*, vol. 69, no. 7, pp. 7930–7939, Jul. 2020.
[64] J. Zhang, Z. Tang, M. Li, D. Fang, P. Nurmi, and Z. Wang, "CrossSense: Towards cross-site and large-scale WiFi sensing," in *Proc. MobiCom*, New Delhi, India, Oct. 2018, pp. 305–320.
[65] H. Abdelnasser, K. Harras, and M. Youssef, "A ubiquitous WiFi-based fine-grained gesture recognition system," *IEEE Trans. Mobile Comput.*, vol. 18, no. 11, pp. 2474–2487, Nov. 2019.
[66] S. Q. Liu, J. C. Zhang, G. Z. Li, and R. Zhu, "A wearable flow-MIMU device for monitoring human dynamic motion," *IEEE Trans. Neural Syst. Rehabil. Eng.*, vol. 28, no. 3, pp. 637–645, Mar. 2020.
[67] K. Ali, A. X. Liu, W. Wang, and M. Shahzad, "Keystroke recognition using WiFi signals," in *Proc. 21st Annu. Int. Conf. Mobile Comput. Netw.*, Sep. 2015, pp. 90–102.
[68] D. Zhang, J. Wang, J. Jang, J. Zhang, and S. Kumar, "On the feasibility of Wi-Fi based material sensing," in *Proc. 25th Annu. Int. Conf. Mobile Comput. Netw.*, Oct. 2019, p. 41.
[69] K. Ohara, T. Maekawa, and Y. Matsushita, "Detecting state changes of indoor everyday objects using Wi-Fi channel state information," in *Proc. ACM Interactive, Mobile, Wearable Ubiquitous Technol.*, Sep. 2017, pp. 88:1–88:28.
[70] J. Ding and R. Chandra, "Towards low cost soil sensing using Wi-Fi," in *Proc. 25th Annu. Int. Conf. Mobile Comput. Netw.*, Oct. 2019, p. 39.
[71] T. Fukushima, T. Murakami, H. Abeysekera, S. Saruwatari, and T. Watanabe, "Evaluating indoor localization performance on an IEEE 802.11ac explicit-feedback-based CSI learning system," in *Proc. IEEE 89th Veh. Technol. Conf. (VTC-Spring)*, Apr. 2019, pp. 1–6.
[72] T. Murakami, M. Miyazaki, S. Ishida, and A. Fukuda, "Wireless LAN-based CSI monitoring system for object detection," *Electronics*, vol. 7, no. 11, p. 290, Nov. 2018.
[73] K. Wu, W. Ni, T. Su, R. P. Liu, and Y. J. Guo, "Expeditious estimation of angle-of-arrival for hybrid Butler matrix arrays," *IEEE Trans. Wireless Commun.*, vol. 18, no. 4, pp. 2170–2185, Apr. 2019.
[74] X. Song, S. Haghighatshoar, and G. Caire, "Efficient beam alignment for millimeter wave single-carrier systems with hybrid MIMO transceivers," *IEEE Trans. Wireless Commun.*, vol. 18, no. 3, pp. 1518–1533, Jan. 2019.
[75] D. Zhang, Y. Hu, Y. Chen, and B. Zeng, "BreathTrack: Tracking indoor human breath status via commodity WiFi," *IEEE Internet Things J.*, vol. 6, no. 2, pp. 3899–3911, Apr. 2019.
[76] J. R. Jiang, C. M. Lin, F. Y. Lin, and S. T. Huang, "ALRD: AoA localization with RSSI differences of directional antennas for wireless sensor networks," *Int. J. Distrib. Sensor Netw.*, vol. 9, no. 3, pp. 1–10, Mar. 2013.
[77] J. Wang, Z. Tian, X. Yang, and M. Zhou, "CSI component reconstruction-based AoA estimation for subtle human-induced reflection under the TTW scenario," *IEEE Commun. Lett.*, vol. 23, no. 8, pp. 1393–1396, Aug. 2019.
[78] H. Tian and L. Zhu, "MIMO CSI-based super-resolution AoA estimation for Wi-Fi indoor localization," in *Proc. 12th Int. Conf. Mach. Learn. Comput.*, Feb. 2020, pp. 457–461.
[79] L. Zhang and H. Wang, "Device-free tracking via joint velocity and AOA estimation with commodity WiFi," *IEEE Sensors J.*, vol. 19, no. 22, pp. 10662–10673, Nov. 2019.
[80] V. Krishnaveni, T. Kesavamurthy, and B. Aparna, "Beamforming for direction-of-arrival (DOA) estimation a survey," *Int. J. Comput. Appl.*, vol. 61, no. 11, pp. 1–11, Jan. 2013.
[81] *IEEE Standard for Information Technology–Telecommunications and Information Exchange Between Systems Local and Metropolitan Area Networks—Specific Requirements—Part 11: Wireless LAN Medium Access Control (MAC) and Physical Layer (PHY) Specifications*, Standard 802.11-2016 (Revision of IEEE Std 802.11-2012), Dec. 2016, pp. 1–3534.

TAKERU FUKUSHIMA (Member, IEEE) received the B.E. and M.E. degrees from Osaka University, Japan, in 2018 and 2020, respectively. He is currently working with NTT Corporation, Access Network Service Systems Laboratories. His current research interests include 5G new radio and other unlicensed wireless access networks. He is a member of IEICE.

TOMOKI MURAKAMI (Member, IEEE) received the B.E., M.E., and Dr. (Eng.) degrees from Waseda University, Japan, in 2006, 2008, and 2015, respectively. In 2008, he joined the NTT Network Innovation Laboratories, Nippon Telegraph and Telephone Corporation (NTT), Yokosuka, Japan. He is currently a Research Engineer with Access Network Systems Laboratories. His current research interest includes high efficiency technologies for future wireless systems. He is a member of IEICE. He received the Young Engineer Award from the IEICE, in 2010, the Active Research Award from IEICE Antenna and Propagation (AP), in 2010, the Best Tutorial Paper Award from IEICE Communications Society, in 2014, the Best Paper Award and the KIYASU-Zen'iti Award from the IEICE, in 2015, and the Best Paper Award from IEICE on AP, in 2016.

HIRANTHA ABEYSEKERA (Member, IEEE) received the B.Eng., M.Eng., and Ph.D. degrees in communications engineering from Osaka University, Japan, in 2005, 2007, and 2010, respectively. He joined the NTT Network Innovation Laboratories, Yokosuka, Japan in 2010, where he was involved in the research and development of next-generation wireless LAN systems. He is currently working as a Senior Research Engineer with the Access Network Service Systems Laboratories, NTT Corporation. His research interest includes resource allocation in wireless LANs. He received the IEEE VTS Japan Student Paper Award, in 2009.

TAKUYA FUJIHASHI (Member, IEEE) received the B.E. and M.S. degrees from Shizuoka University, Japan, in 2012 and 2013, respectively, and the Ph.D. degree from the Graduate School of Information Science and Technology, Osaka University, Japan, in 2016. He has been an Assistant Professor with the Graduate School of Information Science and Technology, Osaka University, since April, 2019. He was a Research Fellow (PD) of the Japan Society for the Promotion of Science, in 2016. From 2014 to 2016, he was a Research Fellow (DC1) of the Japan Society for the Promotion of Science. From 2014 to 2015, he was an Intern with the Mitsubishi Electric Research Laboratories (MERL), Electronics and Communications Group. His research interests include the area of video compression and communications, with a focus on immersive video coding and streaming.

TAKASHI WATANABE (Member, IEEE) received the B.E., M.E., and Ph.D. degrees from Osaka University, Japan, in 1982, 1984, and 1987, respectively. He is currently a Professor with the Graduate School of Information Science and Technology, Osaka University, Japan. He joined the Faculty of Engineering, Tokushima University, as an Assistant Professor, in 1987, and moved to the Faculty of Engineering, Shizuoka University, in 1990. He was a Visiting Researcher with the University of California at Irvine, Irvine, from 1995 to 1996. He has served on many program committees for networking conferences, IEEE, ACM, IPSJ, and IEICE (The Institute of Electronics, Information and Communication Engineers, Japan). His research interests include mobile networking, *ad hoc* networks, sensor networks, ubiquitous networks, and intelligent transport systems, specially MAC and routing. He is a member of IEEE Communications Society, IEEE Computer Society, and IPSJ and IEICE.

SHUNSUKE SARUWATARI (Member, IEEE) received the Doctor of Science degree from The University of Tokyo, in 2007. From 2007 to 2008, he was a Visiting Researcher with the Illinois Genetic Algorithm Laboratory, University of Illinois at Urbana–Champaign. From 2008 to 2012, he was a Research Associate with RCAST, The University of Tokyo. From 2012 to 2016, he was an Assistant Professor with Shizuoka University. He has been an Associate Professor with Osaka University, since 2016. His research interests include the area of wireless networks, sensor networks, and system software.